Quantitative Understanding of Liquid Dynamics at Interfaces from a Free-Energy Landscape Perspective

Simon Hefner, Robin Horstmann⬤, Sebastian Kloth, and Michael Vogel⬤[*]

Institute for Condensed Matter Physics, Technische Universität Darmstadt, Hochschulstraße 6, 64289 Darmstadt, Germany

On the basis of molecular dynamics simulations of water and ethanol in nanopores, we devise a methodology to determine the free-energy landscape (FEL) imposed by an interface on an adjoining liquid directly from the particle trajectories. The methodology merely uses the statistical mechanical relation between occupancy and energy and, hence, is particularly suitable in complex situations, e.g., for disordered or rough atomistic interfaces and molecular liquids, as encountered in many biological, geological, and technological situations. Moreover, we show that the thus-obtained FEL enables a quantitative understanding of interface effects on liquid dynamics. Specifically, by determining the local minima and barriers of the FEL and using an Arrhenius-like relation, we reproduce the very strong spatial variation of the structural relaxation time of water and ethanol across nanopores over a broad temperature range. We anticipate that the proposed FEL approach is transferable to various other liquids and interfaces.

Liquids at interfaces are of outstanding importance [1,2]. For instance, water around biomolecules plays a key role in life's machinery [3–6]. Moreover, many chemical, geological, and technological processes involve water at various kinds of interfaces [6–9]. Further striking examples include polymer melts in composites and films [10–12] or ionic liquids in energy conversion and storage devices [13,14]. In view of this enormous significance, liquids near molecular, soft, or solid surfaces are intensively researched. It is well established that thermodynamics, structures, and dynamics of interfacial liquids and, thus, of severely confined liquids often strongly deviate from those of the bulk counterparts [15–20]. Nevertheless, the effects of interfaces on liquid behaviors remain incompletely understood to this day.

Molecular dynamics (MD) simulations proved to be very suitable to determine properties of liquids at interfaces and in confinements. To gain fundamental insights, several studies [21–26] used simple liquids consisting of, e.g., (quasi) hard spheres or dumbbell-shaped molecules, together with idealized interfaces, like hard smooth walls. In such situations, altered liquid dynamics near interfaces were successfully traced back to different "glassy structural order," i.e., different interparticle correlations [24]. Alternatively, dynamical and thermodynamical properties were linked; e.g., intimate relations between diffusion coefficients and excess entropy or heat capacity were proposed [21,22,26]. However, it was conceded that such relations should break down for self-associating or network-forming liquids like water and ethanol [26].

In theoretical works, mode coupling theory [27] and elastically collective nonlinear Langevin equation (ECNLE) theory [28–30] were extended to situations at interfaces or in confinements. The former approach considered a particular class of confined systems, the "quenched-annealed" mixtures, and predicted different types of glass transition scenarios [27]. The latter approach investigated how mobility changes are nucleated at different types of interfaces and propagated into the interior of the liquid, leading to predictions for the degree, range, and shape of mobility gradients near interfaces [28–30]. In particular, ECNLE theory provided a rationale for a double exponential form frequently observed for the dependence of the structural relaxation time τ on the distance from the interface [25,31,32].

Here, we show that a free-energy landscape (FEL) perspective enables a quantitative understanding of liquid dynamics at interfaces in chemically realistic situations. Specifically, we perform MD simulations for water and ethanol in different types of nanopores with rough solid walls. In analogy to the calculation of a potential of mean force (PMF) [33,34], we compute the time-averaged free energy associated with the interaction between the wall atoms and a liquid molecule, more precisely, a water or ethanol oxygen, in dependence on the position within the pore volume. In other words, we obtain the static FEL imposed by a solid wall on an adjacent liquid. Further determining the local minima and characteristic barriers in this landscape, we successfully predict the very strong variation of the structural relaxation time τ of both liquids across the nanopores in a broad temperature range.

In detail, we simulate models of water (TIP4P/2005 [35]) or ethanol (OPLS-AA [36]) in cylindrical silica or neutral

---
[*]Contact author: michael.vogel@pkm.tu-darmstadt.de

confinements. The silica confinement is modeled using an established force field [37]. Following previous works [32,38,39], it was generated by cutting a cylindrical pore with a radius of 2 nm out of a bulk silica glass, which was obtained from cooling an equilibrated silica melt, and repairing artificially broken bonds by adding hydroxy groups to unsaturated silicon atoms, which led to 4.9 silanol groups per nm^2 on a rough pore wall; see Supplemental Material (Figs. S1 and S2) [40]. For a realistic filling, we determined the number of required water and ethanol molecules by adding liquid reservoirs at both pore ends and simulating these systems at 300 K and 1 bar until equilibration was complete. The term "neutral" refers to the situation that confining matrix and confined liquid consist of the same type of molecules so that the interactions across the interface do not differ from those within the liquid [41–45]. We achieve such a situation for water. For this, we utilize a bulk water system, which was equilibrated at 300 K and 1 bar, and restrain the positions of all oxygen atoms at distances larger than 2 nm from an axis through the center of the simulation box by additional harmonic potentials with a spring constant of 10^6 kJ/mol $\cdot$ nm^{-2}, while the interactions of all other atoms remain unchanged. We determined that, consistent with previous results [32], the wall effects become slightly weaker when the spring constant is decreased to 10^4 kJ/mol $\cdot$ nm^{-2} and, hence, the stiffness of the pore wall is reduced, while the following conclusions are not affected. When performing simulations at various temperatures, we keep the volumes of the thus-generated silica and neutral systems and their particle numbers fixed so as to ensure identical confinement conditions in all analyses, but we observe sufficient equilibration periods prior to the production runs, which have lengths of up to 1 μs, depending on the temperature. For the MD simulations, we use the GROMACS [46,47] simulation package (version 2021.6) and apply periodic boundary conditions. The particle-mesh-Ewald method [48] is employed to calculate Coulomb and Lennard-Jones interactions, while temperature and, during equilibration, pressure are set with the velocity-rescaling thermostat [49] and Parrinello-Rahman barostat [50]. A time step of 2 fs is used for the simulations of the silica confinement, while a smaller value of 0.5 fs is required for the neutral confinement to stabilize temperature in the presence of the additional harmonic potentials.

We start our study by analyzing the spatial variation of water dynamics across the neutral and silica pores. For this purpose, we distinguish between water oxygens residing at various distances R (±0.05 nm) from the pore axis at the time origin t_0 and calculate their respective position-resolved incoherent scattering functions:

$$S_q(t;R) = \left\langle \frac{\sin\left(q|\vec{r}_i(t+t_0) - \vec{r}_i(t_0)|\right)}{q|\vec{r}_i(t+t_0) - \vec{r}_i(t_0)|} \right\rangle_R. \quad (1)$$

Here, $\vec{r}_i(t)$ are the trajectories of the respective fraction of oxygens, the pointed brackets $\langle\cdots\rangle$ indicate ensemble and time (t_0) averaging, and $q = 22.77$ nm^{-1} ensures that displacements on a length scale corresponding to the nearest-neighbor distance and, thus, structural relaxation are observed. We ensured that the exact value of q is not critical, but the use of much larger values would enhance disturbing contributions from vibrational motion, while the results for much smaller values would report on larger displacements, which involve a crossing of several barriers in the FEL determined below, resulting in averaging and blurring of dynamics-energy relations to be established. Using the criterion $S_q(t = \tau; R) = e^{-1}$, we determine position-dependent correlation times $\tau(R)$. Figure 1 shows these dynamical profiles $\tau(R)$ for water in the neutral and silica pores and a broad temperature range. The neutral and silica walls cause strong slowdowns of water dynamics in their vicinity, in particular, at lower temperatures. Specifically, the structural relaxation of water is nearly 2 orders of magnitude slower at both pore walls than in the pore centers and the gradient of $\tau(R)$ extends over ca. 1 nm below 230 K. These findings are in harmony with previous results for water in various atomistically rough confinements [32,41–45,51]. In Supplemental Material (Fig. S3) [40], results from an analogous analysis for ethanol in the silica pore reveal an even stronger slowdown near the pore wall. It amounts to almost 3 orders of magnitude at 280 K.

In the following, we relate the observed gradients in liquid dynamics to the FEL imposed by the wall atoms on the liquid molecules. Along the lines of PMF studies [33,34], we first analyze spatial fluctuations in the time-averaged probability of finding a liquid molecule at a particular position. To this end, we divide the simulation box into cubic voxels with a volume of $(0.05$ nm$)^3$ and
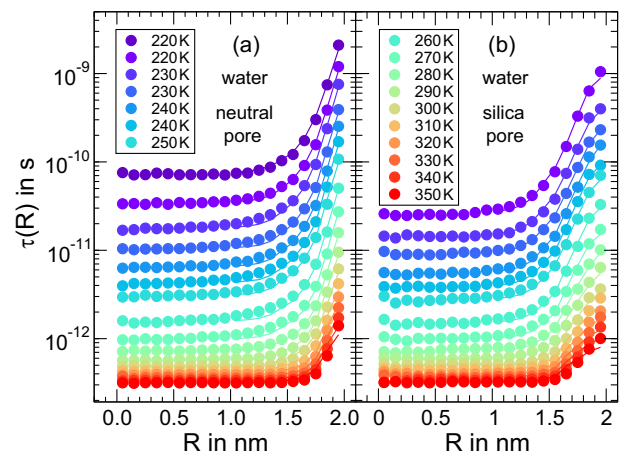

FIG. 1. Correlation time τ of water dynamics as a function of the distance R from the pore axis at various temperatures: (a) neutral pore and (b) silica pore. The points are obtained from $S_q(t = \tau; R) = e^{-1}$, while the lines are fits with the FEL prediction; see Eq. (5).
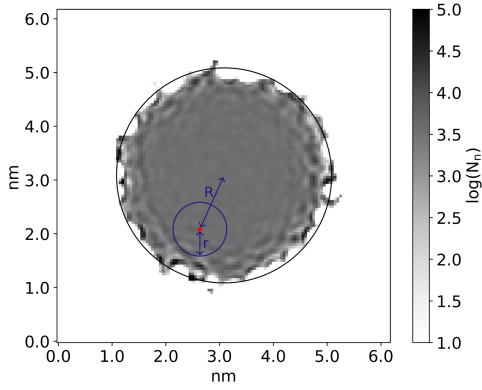
FIG. 2. Occupancies N_n of voxels in an exemplary slice through the neutral pore at 240 K. More frequently occupied voxels are drawn darker. The meaning of the distances R and r is illustrated for the red-colored voxel, which represents a local maximum of the occupancy and, thus, a local minimum of the energy.

determine their occupancies N_n by a liquid molecule. More precisely, N_n is the number of configurations in which voxel n is occupied by any of the liquids' oxygen atoms during the simulated trajectory. The chosen voxel size is a compromise between spatial resolution and statistical uncertainty, but we determined that our conclusions do not critically depend on the specific value.

In Fig. 2, we display the occupancies N_n of the voxels in an exemplary slice through the neutral pore at 240 K. While the N_n values are similar for voxels in the pore center, the occupancies show strong spatial fluctuations near the pore wall. These findings indicate that, in the vicinity of the fixed wall atoms, translational invariance is broken, and favored and unfavored positions exist for the water molecules. For example, the occupancy is high for voxels, which allow for hydrogen bonds between a water molecule and a wall atom, while it is low for voxels between such adsorption sites, in particular, when their distance is small and excluded volume effects play a role. Accordingly, further analysis for water in the silica pore reveals a positive correlation between the preference for a voxel and the capability for hydrogen bonding at this location; see Supplemental Material (Fig. S4) [40]. Thus, the occupancy N_n reflects the time-averaged interaction between a liquid molecule in voxel n and all wall atoms.

To obtain the FEL associated with the wall-liquid interactions, we exploit that the ratio of the occupancies of two voxels m and n, N_m/N_n, is related to the difference of the free energy in these regions, $E_m - E_n$ [33,34]:

$$E_m - E_n = -k_B T \ln(N_m/N_n). \qquad (2)$$

This knowledge about the free-energy differences allows us to determine the local minima in the landscape. Explicitly, we identify the voxels $n_{\min}$, which have smaller free energies $E_n^{\min}$ than all of the 26 surrounding voxels.

Having localized the local FEL minima, we extract characteristic values of their depth depending on their position within the pore. Specifically, for all local minima, we calculate the mean difference $\Delta\varepsilon(r)$ between the energies E_m of all voxels m located at a distance r from the respective $n_{\min}$ and $E_n^{\min}$ (see Fig. 2). Then, we average the $\Delta\varepsilon(r)$ results of all local minima $n_{\min}$ at a distance R from the pore axis. Strictly speaking, we calculate

$$\Delta\varepsilon(r; R) = \langle\langle E_m - E_n^{\min}\rangle_{m@r}\rangle_{n_{\min}@R}. \qquad (3)$$

Here, the distances r and R are calculated based on the positions of the voxel centers, $\langle\cdots\rangle_{m@r}$ indicates the average over all voxels m at distance r (± 0.025 nm) from voxel $n_{\min}$, and $\langle\cdots\rangle_{n_{\min}@R}$ means the average over all voxels $n_{\min}$ at distance R (± 0.05 nm) from the pore axis.

Figure 3(a) shows the mean energy differences $\Delta\varepsilon(r; R)$ obtained for water in the neutral pore at 220 K. In the pore center ($R < 1$ nm), $\Delta\varepsilon(r)$ is small and reflects essentially statistical fluctuations. When moving radially outward, the energy differences increase, indicating that the FEL becomes rougher. At the pore wall ($R \to 2$ nm), $\Delta\varepsilon(r)$ is maximum at $r \approx 0.16$ nm, which is slightly larger than half the oxygen-oxygen nearest-neighbor distance in liquid water. This finding implies that

$$\varepsilon_B(R) \equiv \Delta\varepsilon(r = 0.16 \text{ nm}; R) \qquad (4)$$

can be considered as the typical height of the energy barriers between FEL minima. In Supplemental Material (Fig. S5) [40], an analogous analyses for water in the silica pore yields qualitatively similar results for $\Delta\varepsilon(r; R)$.

In Fig. 3(b), we display the energy barriers $\varepsilon_B(R)$ for water in the neutral pore at various temperatures. We find that the energy barriers are small and constant in the pore
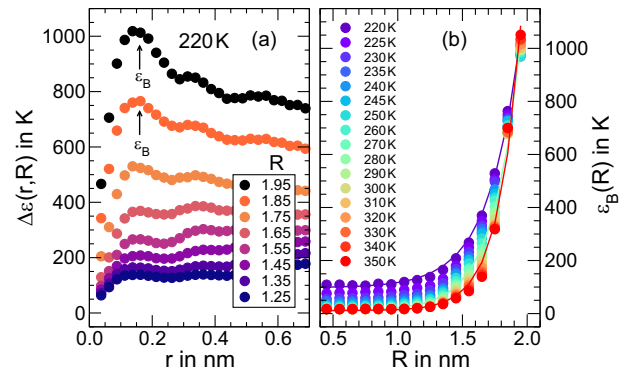

FIG. 3. Characterization of the FEL in the neutral pore. (a) Mean energy difference $\Delta\varepsilon$ with respect to a minimum at a distance r for the indicated locations R at 220 K. The arrows mark the position of the energy barriers; see Eq. (4). (b) Energy barriers ε_B as a function of the distance R from the pore axis at the indicated temperatures. The lines are exemplary exponential fits; see Supplemental Material [40].

center but increase approximately exponentially when approaching the pore wall, where they reach notable values of $\varepsilon_B \sim 1000$ K. While the constant value in the pore center is a result of remaining statistical uncertainty, the exponential dependence of the energy barriers on the distance from the interface, which is more clearly seen in a semilogarithmic representation in Supplemental Material (Fig. S6) [40], is consistent with arguments on the basis of ECNLE theory [28–30]. Moreover, when we assume thermally activated motion, such variation of ε_B across the pore provides a rationale for the observed double exponential distance dependence of the structural relaxation time τ [25,31,32]. We expect that our analyses at various temperatures do not produce identical results for $\varepsilon_B(R)$ because, at lower temperatures, the atoms show lower mobility and the hydrogen-bond network has higher tetrahedral order so that the FEL is less smeared by thermal motion and effects generated at the interface are more effectively passed between various "water layers" near the wall. In Supplemental Material [40], we show that, different from our findings for the neutral pore, $\varepsilon_B(R)$ does not show an exponential distance dependence for water and ethanol in the silica pore (Figs. S7 and S8). We attribute this difference to the fact that, unlike near neutral walls, the hydrogen-bond networks and, thus, liquid-liquid interactions are strongly altered near silica walls (see below).

To finally relate energetics and dynamics, we assume that an underlying static energy landscape impedes typical liquidlike molecular rearrangements, e.g., small displacements, which facilitate or accommodate structural relaxation events like cage escape. In this way, it causes slower and more jumplike dynamics. Based on these arguments, we propose that energy barriers, corrected for their statistical value in the pore center, and dynamical profiles are related in an Arrhenius-type fashion:

$$\frac{\tau(R,T)}{\tau(R \to 0, T)} = \exp\left[\frac{[\varepsilon_B(R) - \varepsilon_B(R \to 0)]s(T)}{k_B T}\right]. \quad (5)$$

Here, $s(T)$ is a fit parameter, which scales the energy barriers, if required, as discussed below. Revisiting Fig. 1, we observe that all dynamical profiles $\tau(R)$ of confined water are well described when using $\varepsilon_B(R)$ in Eq. (5). In particular, the different curvature of $\tau(R)$ in the immediate vicinity of neutral and silica walls is reproduced. In Supplemental Material (Fig. S3) [40], it is shown that the even stronger mobility gradient of ethanol in the silica pore is also attributable to the wall-imposed FEL.

The scaling factors $s(T)$ obtained from these fits for water in the neutral and silica pores are shown in Fig. 4(a). For the neutral pore at 230–270 K, the analysis yields $s > 0.9$, and, hence, the strong slowdown of water dynamics upon approaching the interface can be understood almost completely based on the energy barriers $\varepsilon_B(R)$. Above 270 K, the value of s decreases with increasing
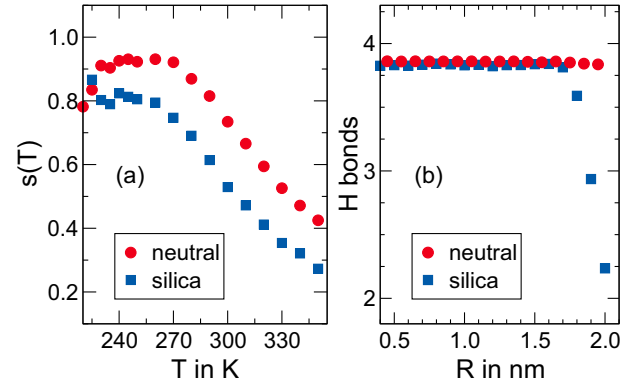

FIG. 4. (a) Scaling factor $s(T)$ of the energy barriers $\varepsilon_B(R)$ obtained from fitting $\tau(R,T)$ of the neutral and silica pores with Eq. (5). (b) Mean number of hydrogen bonds of a water molecule at a distance R from the pore axis at 250 K. In this analysis, the hydrogen bonds were identified on the basis of the widely used geometrical criterion [53,54].

temperature, implying that the energy barriers and activated motion become less relevant. Below 230 K, the tetrahedral order of the liquid increases when the second critical point ($T_c = 193$ K [52]) of the water model is approached, while that of the wall remains unaltered and, hence, the wall becomes "non-neutral," approaching the situation for the silica pore. For the latter, the scaling factor amounts to $s \approx 0.8$ at $T \leq 270$ K. To rationalize this smaller value, we need to consider that water dynamics are also affected by distortions in the hydrogen-bond network. Figure 4(b) shows the mean number of hydrogen bonds of a water molecule at a distance R from the axis of the neutral and silica pores at 250 K. The number of hydrogen bonds is hardly altered near the neutral wall, whereas it strongly decreases near the silica wall. The undisturbed hydrogen-bond network goes along with $s \to 1$ in the neutral pore at ~250 K. The distorted water structure at the silica wall would lead to faster water dynamics if this was the only interface effect. However, this speedup is overcompensated by the slowdown described by Eq. (5). Thus, the counteracting effect of the distorted water structure weakens the effect of the FEL, which manifests itself in a downscaling of the barrier heights. Therefore, we speculate that the scaling factor s can be taken as a measure to which degree liquid structures are distorted ($s < 1$) or strengthened ($s > 1$) at interfaces. This information is difficult to obtain otherwise, because common structure identifiers are trivially altered by the mere fact that the number of neighbors is reduced due to excluded volume caused by the wall.

In summary, we devised a methodology to determine the FEL imposed by an interface on an adjoining liquid from an MD simulation trajectory. The methodology does not involve an explicit calculation of interaction energies but uses the statistical mechanical relation between occupancy and energy, and, hence, it is not limited to simple situations where energy calculations are straightforward. Rather, it

allows one to consider the effects of disordered and rough atomistic interfaces on molecular liquids, which are highly relevant in many biological, geological, and technological situations. Beyond that, we showed that the thus-determined FEL enables a quantitative understanding of interface effects on liquid dynamics. Specifically, determining the local minima and barriers of the FEL and using an Arrhenius-like relation, we reproduced the spatial variation of the structural relaxation time in nanopores. We anticipate that the proposed approach is transferable to further liquids and confinements. In the special case of soft interfaces, we expect it to work on timescales between those of the faster structural relaxation of the liquid and the slower structural reorganization of the wall.

[1] J. N. Israelachvili, *Intermolecular and Surface Forces* (Academic Press, Amsterdam, 2011).

[2] H.-J. Butt, K. Graf, and M. Kappl, *Physics and Chemistry of Interfaces* (John Wiley & Sons, Weinheim, 2013).

[3] M. Chaplin, Nat. Rev. Mol. Cell Biol. **7**, 861 (2006).

[4] P. Ball, Chem. Rev. **108**, 74 (2008).

[5] M.-C. Bellissent-Funel, A. Hassanali, M. Havenith, R. Henchman, P. Pohl, F. Sterpone, D. van der Spoel, Y. Xu, and A. E. Garcia, Chem. Rev. **116**, 7673 (2016).

[6] B. Bagchi, *Water in Biological and Chemical Processes: From Stucture and Dynamics to Function* (Cambridge University Press, Cambridge, England, 2013).

[7] O. Björneholm, M. H. Hansen, A. Hodgson, L.-M. Liu, D. T. Limmer, A. Michaelides, P. Pedevilla, J. Rossmeisl, H. Shen, G. Tocci, E. Tyrode, M.-M. Walz, J. Werner, and H. Bluhm, Chem. Rev. **116**, 7698 (2016).

[8] G. Gonella, E. H. G. Backus, Y. Nagata, D. J. Bonthuis, P. Loche, A. Schlaich, R. R. Netz, A. Kühnle, I. T. McCrum, M. T. M. Koper, M. Wolf, B. Winter, G. Meijer, R. Kramer Campen, and M. Bonn, Nat. Rev. Chem. **5**, 466 (2021).

[9] L. Chen and L. Qian, Friction **9**, 1 (2021).

[10] S. Napolitano, E. Glynos, and N. B. Tito, Rep. Prog. Phys. **80**, 036602 (2017).

[11] M. A. Kashfipour, N. Mehra, and J. Zhu, Adv. Compos. Hybrid Mater. **1**, 415 (2018).

[12] *Polymer Films: Properties, Performance and Applications*, edited by S. A. Romano and G. P. Somners (Nova Science Publishers Inc., Hauppauge, 2011).

[13] R. Hayes, G. G. Warr, and R. Atkin, Chem. Rev. **115**, 6357 (2015).

[14] M. Watanabe, M. L. Thomas, S. Zhang, K. Ueno, T. Yasuda, and K. Dokko, Chem. Rev. **117**, 7190 (2017).

[15] M. Alcoutlabi and G. B. McKenna, J. Phys. Condens. Matter **17**, R461 (2005).

[16] M. Vogel, Eur. Phys. J. Special Topics **189**, 47 (2010).

[17] R. Richert, Annu. Rev. Phys. Chem. **62**, 65 (2011).

[18] F. Kremer, ed., *Dynamics in Geometrical Confinement* (Springer, Heidelberg, 2014).

[19] P. Huber, J. Phys. Condens. Matter **27**, 103102 (2015).

[20] W. H. Thompson, J. Chem. Phys. **149**, 170901 (2018).

[21] J. Mittal, J. R. Errington, and T. M. Truskett, Phys. Rev. Lett. **96**, 177804 (2006).

[22] J. Mittal, T. M. Truskett, J. R. Errington, and G. Hummer, Phys. Rev. Lett. **100**, 145901 (2008).

[23] J. Kurzidim, D. Coslovich, and G. Kahl, Phys. Rev. Lett. **103**, 138303 (2009).

[24] K. Watanabe, T. Kawasaki, and H. Tanaka, Nat. Mater. **10**, 512 (2011).

[25] W. Kob, S. Roldán-Vargas, and L. Berthier, Nat. Phys. **8**, 164 (2012).

[26] T. S. Ingebrigtsen, J. R. Errington, T. M. Truskett, and J. C. Dyre, Phys. Rev. Lett. **111**, 235901 (2013).

[27] V. Krakoviack, Phys. Rev. Lett. **94**, 065703 (2005).

[28] A. D. Phan and K. S. Schweizer, J. Chem. Phys. **150**, 044508 (2019).

[29] K. S. Schweizer and D. S. Simmons, J. Chem. Phys. **151**, 240901 (2019).

[30] A. D. Phan and K. S. Schweizer, ACS Macro Lett. **9**, 448 (2020).

[31] P. Scheidler, W. Kob, and K. Binder, J. Phys. Chem. B **108**, 6673 (2004).

[32] R. Horstmann, L. Hecht, S. Kloth, and M. Vogel, Langmuir **38**, 6506 (2022).

[33] B. Roux, Comput. Phys. Commun. **91**, 275 (1995).

[34] D. Trzesniak, A.-P. E. Kunz, and W. F. van Gunsteren, ChemPhysChem **8**, 162 (2007).

[35] J. L. F. Abascal and C. Vega, J. Chem. Phys. **123**, 234505 (2005).

[36] W. L. Jorgensen and D. S. Maxwell and J. Tirado-Rives, J. Am. Chem. Soc. **118**, 11225 (1996).

[37] F. S. Emami, V. Puddu, R. J. Berry, V. Varshney, S. V. Patwardhan, C. C. Perry, and H. Heinz, Chem. Mater. **26**, 2647 (2014).

[38] J. Geske, B. Drossel, and M. Vogel, Mol. Simul. **43**, 13 (2017).

[39] R. Köster and M. Vogel, J. Chem. Phys. **156**, 074501 (2022).

[40] See Supplemental Material at http://link.aps.org/supplemental/10.1103/PhysRevLett.133.106201 for snapshots of the used confinements, density profiles, spatially resolved analyses for ethanol in the silica pore, the relation between hydrogen bonding and site occupancy, the FEL of water in the silica pore, and semilogarithmic representations of position-dependent energy barriers.

[41] F. Klameth and M. Vogel, J. Chem. Phys. **138**, 134503 (2013).

[42] F. Klameth, P. Henritzi, and M. Vogel, J. Chem. Phys. **140**, 144501 (2014).

[43] F. Klameth and M. Vogel, J. Phys. Chem. Lett. **6**, 4385 (2015).

[44] M. F. Harrach, F. Klameth, B. Drossel, and M. Vogel, J. Chem. Phys. **142**, 034703 (2015).

[45] R. Horstmann, E. P. Sanjon, B. Drossel, and M. Vogel, J. Chem. Phys. **150**, 214704 (2019).

[46] D. Van Der Spoel, E. Lindahl, B. Hess, G. Groenhof, A. E. Mark, and H. J. C. Berendsen, J. Comput. Chem. **26**, 1701 (2005).

[47] B. Hess, C. Kutzner, D. van der Spoel, and E. Lindahl, J. Chem. Theory Comput. **4**, 435 (2008).

[48] T. Darden, D. York, and L. Pederson, J. Chem. Phys. **98,** 10089 (1993).

[49] G. Bussi, D. Donadio, and M. Parrinello, J. Chem. Phys. **126,** 014101 (2007).

[50] M. Parrinello and A. Rahman, J. Appl. Phys. **52,** 7182 (1981).

[51] P. Gallo, M. Rovere, and S.-H. Chen, J. Phys. Chem. Lett. **1,** 729 (2010).

[52] J. L. F. Abascal and C. Vega, J. Chem. Phys. **133,** 234502 (2010).

[53] A. Luzar and D. Chandler, Nature (London) **379,** 55 (1996).

[54] D. Laage and J. T. Hynes, Science **311,** 832 (2006).